Organic Electronics 14 (2013) 599–606

Contents lists available at SciVerse ScienceDirect

Organic Electronics

journal homepage: www.elsevier.com/locate/orgel

Evolved structure of thiazolothiazole based small molecules towards enhanced efficiency in organic solar cells

Pei Cheng [a,b], Qinqin Shi [a], Yuze Lin [a,b], Yongfang Li [a], Xiaowei Zhan [a,c,*]

[a] Beijing National Laboratory for Molecular Sciences, Key Laboratory of Organic Solids, Institute of Chemistry, Chinese Academy of Sciences, Beijing 100190, China
[b] University of Chinese Academy of Sciences, Beijing 100049, China
[c] Department of Materials Science and Engineering, College of Engineering, Peking University, Beijing 100871, China

ARTICLE INFO

Article history:
Received 15 October 2012
Received in revised form 21 November 2012
Accepted 25 November 2012
Available online 11 December 2012

Keywords:
Thiazolothiazole
Triphenylamine
Small molecule
Organic solar cell
Solution process
Structure–property relationship

ABSTRACT

Small molecule donors **T0–T2** with thiazolothiazole as acceptor unit, triphenylamine as donor unit and thiophene with different number as bridge are synthesized. With increasing thiophene number and conjugation length, these molecules exhibit red-shifted absorption (300–600 nm), slightly up-shifted HOMO levels (−5.31 to −5.28 eV), slightly down-shifted LUMO levels (−2.64 to −2.75 eV), and reduced optical band gaps (2.55–2.11 eV). Solution processed organic solar cells based on **T0–T2**/$PC_{71}BM$ (1:4, w/w) after thermal annealing exhibit power conversion efficiency up to 2.19%, 3.73% and 4.05% under AM 1.5G illumination (100 mW/cm^2), respectively. Effects of thermal annealing on morphology, charge transport and photovoltaic property of blend films are investigated.

© 2012 Elsevier B.V. All rights reserved.

1. Introduction

Due to traditional energy depletion and environmental pollution, solar cells have attracted considerable attentions. Especially, bulk heterojunction organic solar cells with some advantages such as simple preparation, light weight, low cost and large area flexible fabrication have been the focus of research in the past decade [1–6]. In recent years, design and synthesis of new low-bandgap and high-mobility polymer donor materials, new fullerene derivative acceptor materials, and optimization of device structures have promoted power conversion efficiency (PCE) over 8% for polymer solar cells [7–15].

Compared with polymer solar cells, small molecule based solar cells have advantages in terms of defined molecular structure, accurate molecular weight, easy purification, easy mass-scale production, and good batch-to-batch reproducibility [16–21]. Currently, the PCEs of small molecule based organic solar cells (OSCs) have touched 4–7% [22–30]. Recently, Chen et al. report a PCE over 7% for small molecule based OSCs [31].

Thiazolothiazole is a rigid, coplanar, and electron-accepting fused heterocycle due to electron-withdrawing nitrogen of imine (C=N) [32]. Recently, some thiazolothiazole-based polymers were synthesized for polymer solar cell applications, and PCEs up to 5–6% were reported [33–48]. Relative to thiazolothiazole-based polymers, thiazolothiazole-based small molecule photovoltaic materials remain rare [49–51]. In our previous communication, we have reported a thiazolothiazole-based small molecule, 2,5-bis(5-triphenylamino-3-dodecyl-thiophen-2-yl)-thiazolo[5,4-d]thiazole (**T1**, Fig. 1) [49]. Molecule **T1** exhibits relatively narrow absorption but high PCE (3.73%) in solution processed OSCs, which is potential for semi-transparent solar cells coated on the glasses of buildings. In this work, we report a series of D–A–D molecules with thiazolothiazole as acceptor (A) unit, triphenylamine (TPA) as donor (D) unit and thiophene with different number as bridge (**T0, T1** and **T2**, Fig. 1). We investigate the effects of thiophene number

* Corresponding author at: Beijing National Laboratory for Molecular Sciences, Key Laboratory of Organic Solids, Institute of Chemistry, Chinese Academy of Sciences, Beijing 100190, China.
E-mail address: xwzhan@iccas.ac.cn (X. Zhan).

1566-1199/$ - see front matter © 2012 Elsevier B.V. All rights reserved.
http://dx.doi.org/10.1016/j.orgel.2012.11.026

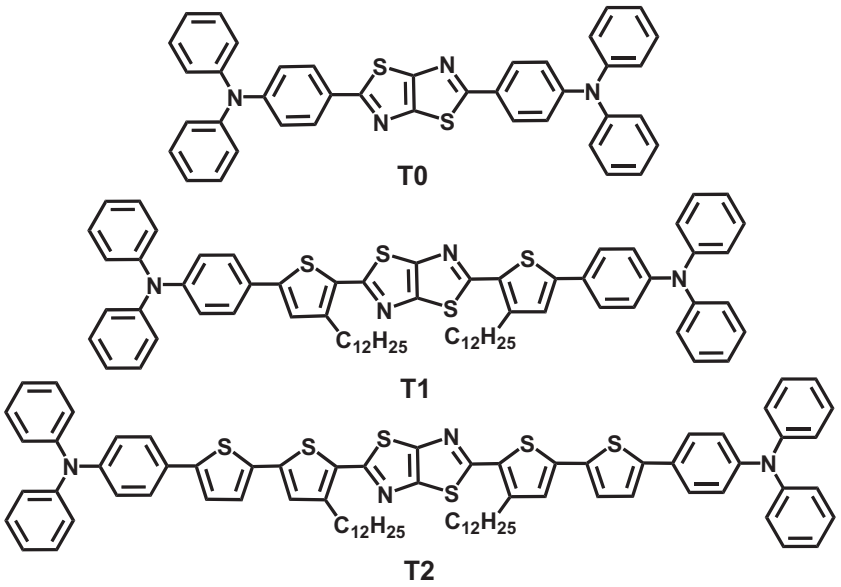

Fig. 1. Molecule structure of **T0**, **T1** and **T2**.

on absorption, energy level, charge transport and photovoltaic properties of the molecules. Solution processed OSCs based on **T2** with 2 thiophene units afford a PCE as high as 4.05% after thermal annealing, which is higher than that based on **T1** and is the highest for thiazole-based small molecule solar cells.

2. Experimental section

2.1. Measurements and characterization

The ^{1}H and ^{13}C NMR spectra were measured on a Bruker AVANCE 400 MHz spectrometer using tetramethylsilane (δ = 0 ppm) as an internal standard. Mass spectra were measured on a GCT–MS micromass spectrometer using the electron impact (EI) mode or on a Bruker Daltonics BIFLEX III MALDI-TOF Analyzer using MALDI mode. Elemental analyses were carried out using a FLASH EA1112 elemental analyzer. Thermogravimetric analysis (TGA) measurements were performed on Shimadzu thermogravimetric analyzer (model DTG-60) under a nitrogen flow at a heating rate of 10 °C/min. Solution (chloroform) and thin-film (on quartz substrate) UV–vis absorption spectra were recorded on a JASCO V-570 spectrophotometer. Electrochemical measurements were carried out under nitrogen in a deoxygenated solution of tetra-*n*-butylammonium hexafluorophosphate (0.1 M) in acetonitrile using a computer-controlled CHI660C electrochemical workstation, a thin film of the sample coated on platinum working electrode, a platinum-wire auxiliary electrode, and an Ag wire anodized with AgCl as a pseudoreference electrode. The nanoscale morphology of blend film was observed by an atomic force microscopy (AFM) (NanoMan VS, Veeco, USA) in contact mode.

2.2. Fabrication and characterization of photovoltaic cells

Organic solar cells were fabricated with ITO as positive electrode and Ca/Al as negative electrode. The patterned indium tin oxide (ITO) glass (sheet resistance = 30 $\Omega\,\square^{-1}$) was pre-cleaned in an ultrasonic bath of acetone and isopropanol, and treated in ultraviolet-ozone chamber (Jelight Company, USA) for 23 min. A thin layer (35 nm) of poly(3,4-ethylenedioxythiophene):poly(styrene sulfonate) (PEDOT:PSS, Baytron P VP AI 4083, Germany) was spin-coated onto the ITO glass and baked at 150 °C for 20 min. A dichlorobenzene solution of blend of compounds **T0**–**T2** with $PC_{71}BM$ (1:2, 1:3 or 1:4, w/w) was subsequently spin-coated on PEDOT:PSS layer to form a photosensitive layer. The thickness (ca. 70–80 nm) of the photosensitive layer was measured by Ambios Technology XP-2 profilometer. A calcium (ca. 15 nm) and aluminum layer (ca. 60 nm) was then evaporated onto the surface of the photosensitive layer under vacuum (ca. 10^{-4} Pa) to form the negative electrode. The active area of the device was 4 mm^2. *J*–*V* curve was measured with a computer-controlled Keithley 236 Source Measure Unit. A xenon lamp coupled with AM 1.5 solar spectrum filters was used as the light source, and the optical power at the sample was 100 mW cm^{-2}. The IPCE spectrum was measured by Stanford Research Systems model SR830 DSP lock-in amplifier coupled with WDG3 monochromator and 500 W xenon lamp. Hole-only or electron-only diodes were fabricated using the architectures: ITO/PEDOT:PSS/**T0**–**T2**:$PC_{71}BM$/Au for holes and Al/**T0**–**T2**:$PC_{71}BM$/Al for electrons. Mobilities were extracted by fitting the current density–voltage curves using the Mott–Gurney relationship (space charge limited current).

2.3. Materials

Unless stated otherwise, starting materials were obtained commercially and were used without further purification. Toluene was distilled from sodium-benzophenone under nitrogen prior to use, DMF was distilled form calcium hydride under nitrogen prior to use. *N*-phenyl-*N*-(4-(5-(tributylstannyl)thiophen-2-yl)phenyl)benzenamine

[52] and 2,5-bis(5-bromo-3-dodecylthiophen-2-yl)-thiazolo[5,4-*d*]thiazole [53] were synthesized according to the literature procedures.

2.4. Synthesis

2.4.1. 4,4′-(Thiazolo[5,4-d]thiazole-2,5-diyl)bis(N,N-diphenylaniline) (T0)

To a three-necked round bottom flask were added 4-(diphenylamino)benzaldehyde (2.8 g, 10.2 mmol), ethanebis(thioamide) (600 mg, 5.0 mmol) and DMF (30 mL). The mixture was deoxygenated with nitrogen for 30 min. The mixture was stirred at 155 °C for 6 h, and then cooled down to room temperature. Water (50 mL) was added and the mixture was extracted with dichloromethane (2 × 150 mL). The organic phase was dried over anhydrous $MgSO_4$ and filtered. After removing the solvent from filtrate, the residue was purified by column chromatography on silica gel using petroleum ether/dichloromethane (1:2) as eluent yielding a yellow solid (630 mg, 20%). ^{1}H NMR (400 MHz, $CDCl_3$): δ 7.80 (d, J = 8.4 Hz, 4H), 7.29 (t, J = 7.8 Hz, 8H), 7.15 (d, J = 8.0 Hz, 8H), 7.10 (d, J = 7.8 Hz, 4H), 7.07 (d, J = 8.0 Hz, 4H). ^{13}C NMR (100 MHz, $CDCl_3$): δ 168.48, 150.30, 150.10, 147.03, 129.63, 127.39, 127.30, 125.46, 124.11, 122.06, HRMS (EI): m/z 628.1760 (calcd. for $C_{40}H_{28}N_4S_2$, 628.1755). Anal. Calcd for $C_{40}H_{28}N_4S_2$: C, 76.40; H, 4.49; N, 8.91. Found: C, 76.12; H, 4.39; N, 8.80%.

2.4.2. 4,4′-(5′,5″-(Thiazolo[5,4-d]thiazole-2,5-diyl)bis(4′-dodecyl-2,2′-bithiophene-5′,5-diyl))bis(N,N-diphenylbenzenamine) (T2)

To a three-necked round bottom flask were added 2,5-bis(5-bromo-3-dodecylthiophen-2-yl)thiazolo[5,4-d]thiazole (120 mg, 0.15 mmol) and *N*-phenyl-*N*-(4-(5-(tributylstannyl)thiophen-2-yl)phenyl)benzenamine (247 mg, 0.4 mmol), and anhydrous toluene (20 mL). The mixture was deoxygenated with nitrogen for 30 min. $Pd(PPh_3)_4$ (23 mg, 0.02 mmol) was added under nitrogen. The mixture was refluxed for 2 d and then cooled down to room temperature. A solution of KF (1 g) in water (10 mL) was added and stirred at room temperature for 2.5 h to remove the tin impurity. Water (100 mL) was added and the mixture was extracted with $CHCl_3$ (2 × 100 mL). The organic phase was dried over anhydrous $MgSO_4$. After removing the solvent, the residue was purified by column chromatography on silica gel using petroleum ether/$CHCl_3$ (10:1) as eluent yielding a red solid (160 mg, 82%). ^{1}H NMR (400 MHz, $CDCl_3$): δ 7.47 (d, J = 6.8 Hz, 4H), 7.30 (t, J = 7.6 Hz, 8H), 7.14 (m, 12H), 7.06 (m, 10H), 2.94 (t, J = 7.6 Hz, 4H), 1.74 (m, 4H), 1.48 (m, 4H), 1.38 (m, 4H), 1.27 (m, 28H), 0.88 (m, 6H). ^{13}C NMR (100 MHz, $CDCl_3$): δ 160.52, 150.05, 147.47, 143.91, 143.60, 138.68, 135.11, 130.36, 129.43, 127.82, 126.40, 126.22, 126.10, 125.40, 124.73, 123.42, 123.32, 123.11, 32.08, 30.66, 30.01, 29.89, 29.70, 29.54, 29.49, 22.84, 14.27. MS (MALDI): m/z 1292.5 (M^+). Anal. Calcd. for $C_{80}H_{84}N_4S_6$: C, 74.26; H, 6.54; N, 4.33. Found: C, 74.39; H, 6.66; N, 4.25%.

3. Results and discussion

3.1. Synthesis and characterization

The synthesis of compound **T1** was reported in our previous paper [49]. Condensation reaction of 4-(diphenylamino)benzaldehyde and ethanebis(thioamide) in DMF afforded **T0** (Scheme 1). Stille coupling reaction of thiazolothiazole-dithiophene dibromide and triphenylamine–thiophene tin yielded **T2**. All compounds were fully characterized by MS, ^{1}H NMR, ^{13}C NMR, and elemental analysis. Compounds **T0**–**T2** are readily soluble in common organic solvents such as dichloromethane, dichlorobenzene and chloroform at room temperature. The thermal properties of **T0**–**T2** were investigated by thermogravimetric analysis (TGA). All compounds have excellent thermal stability with decomposition temperatures (T_d, 5% weight loss) of 355–420 °C (Fig. 2).

3.2. Absorption spectra

The absorption spectra of **T0**–**T2** in dichloromethane solution and in thin film are shown in Fig. 3. With increasing thiophene number and conjugation length, the absorption edge of **T0**–**T2** gradually red shifts and the molar extinction coefficient increases from 2.80×10^4 to 9.40×10^4 M^{-1} cm^{-1}. Relative to **T0** without thiophene bridge, **T1** with one thiophene exhibits broader absorption although its absorption maximum slightly blue shifts. Adding one thiophene to **T1** leads to significant red shift (66 nm) of the absorption maximum and significant enhancement of the molar extinction coefficient. The absorption profile of **T0**–**T2** in thin film is similar to that in solution. The optical band gap (E_g^{opt}) of **T0**–**T2** estimated from the absorption edge in film decreases from 2.55 to 2.11 eV with increasing thiophene number.

3.3. Electrochemistry

To estimate the highest occupied molecular orbital (HOMO) and lowest unoccupied molecular orbital (LUMO) positions of **T0**–**T2**, cyclic voltammetry (CV) was carried out using films on glassy carbon working electrode in 0.1 M $[^nBu_4N]^+[PF_6]^-$ CH_3CN solution at a potential scan rate of 100 mV s^{-1} (Fig. 4). All compounds exhibit irreversible reduction wave and quasi-reversible oxidation wave. The HOMO and LUMO values of compounds **T0**–**T2** are estimated from the onset oxidation and reduction potentials, assuming the absolute energy level of $FeCp_2^{+/0}$ to be 4.8 eV below vacuum. With increasing thiophene number and conjugation length, the HOMO level slightly up-shifts from −5.31 eV to −5.28 eV and the LUMO level slightly down-shifts from −2.64 eV to −2.75 eV due to the delocalization of π electrons (Table 1). Thus, the band gap decreases with increasing thiophene number, which is consistent with the absorption data. The HOMO–LUMO gaps (E_g^{ec}) obtained from electrochemistry are 2.67–2.53 eV, 0.12–0.42 eV larger than the optical band gaps (E_g^{opt}, 2.55–2.11 eV). This phenomenon was also observed

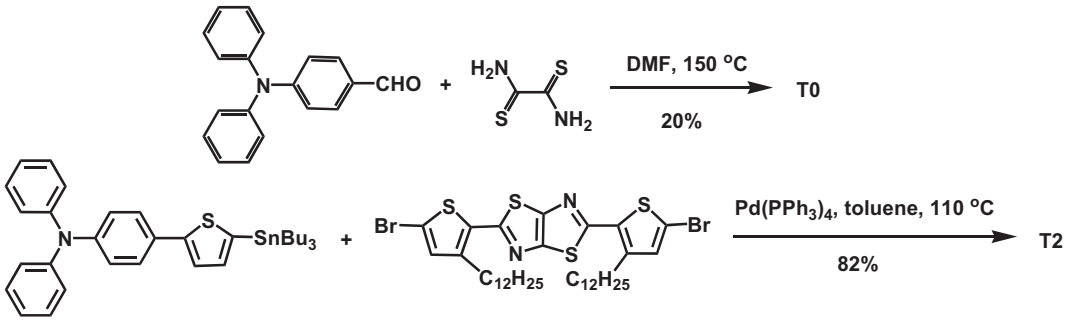

Scheme 1. Synthetic routes to compounds **T0** and **T2**.

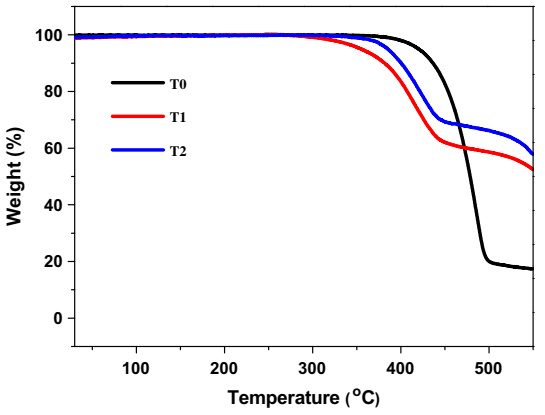

Fig. 2. TGA curves of compounds **T0**–**T2**.

for some thiazolothiazole-based polymers in literatures [38,39].

3.4. Organic solar cells

We used **T0**–**T2** as the donor material, $PC_{71}BM$ as the acceptor material to fabricate bulk heterojunction solar cells. The HOMO energy levels of **T0**–**T2** are down to ca. −5.3 eV, and the difference between HOMO energy level of donor and LUMO energy level of acceptor is ca. 1.4 eV. Such a large difference is beneficial to increasing the open circuit voltage (V_{OC}) [4].

Fig. 5 shows the *J*–*V* and the incident-photon conversion efficiency (IPCE) characteristics of as cast and annealed **T0**–**T2**/$PC_{71}BM$ devices under AM 1.5G illumination at an intensity of 100 mW cm^{-2}. Table 2 shows the average and best device characteristics at different **T0**–**T2**/$PC_{71}BM$ weight ratios without or with thermal annealing at different temperatures. As shown in Table 2, the ratio of donor to acceptor strongly affects the short circuit current density (J_{SC}) but slightly affects the V_{OC} and fill factor (FF). The J_{SC} and PCE increase with increasing ratio of the donor to acceptor. Before thermal annealing, the solar cells exhibit the best performance at the ratio of 1:4; **T0**–**T2**/$PC_{71}BM$ devices exhibit an average PCE of 2.13%, 2.52% and 2.66%, respectively. The PCE increases with increasing thiophene number and conjugation length. The V_{OC} and FF are slightly sensitive to the thiophene number and conjugation length.

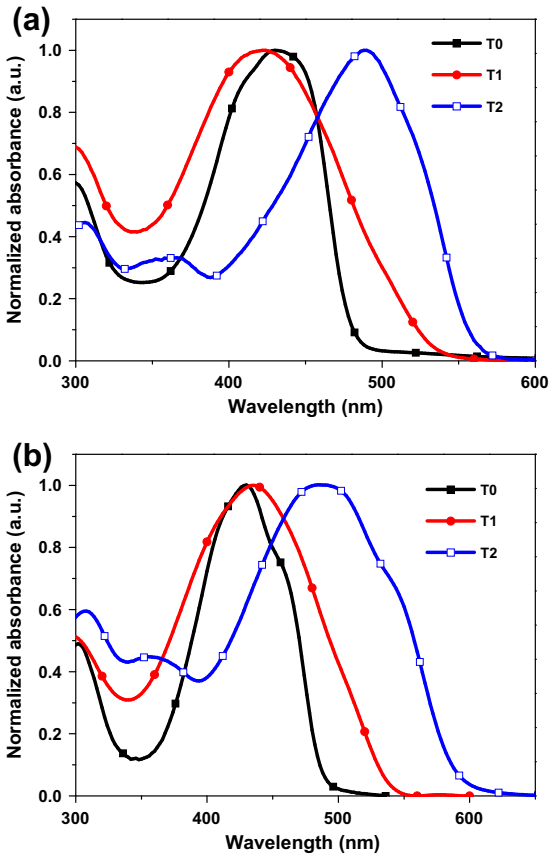

Fig. 3. UV–vis absorption spectra of **T0**–**T2** in dichloromethane solution (a) and in thin film (b).

However, J_{SC} increases with increasing thiophene number and conjugation length, which is consistent with the trend in IPCE and absorption spectra.

Thermal annealing leads to significant performance improvement in **T1** and **T2** based devices, and thermal annealing temperature exerts significant impact on device performance. The average PCE of **T1**/$PC_{71}BM$ (1:4, w/w) devices increase from 2.52% to 3.61% after thermal annealing at 110 °C for 10 min. The **T2**/$PC_{71}BM$ (1:4, w/w) devices exhibit the best performance after annealing at 120 °C for 10 min; the average V_{OC}, J_{SC}, FF and PCE is 0.85 V,

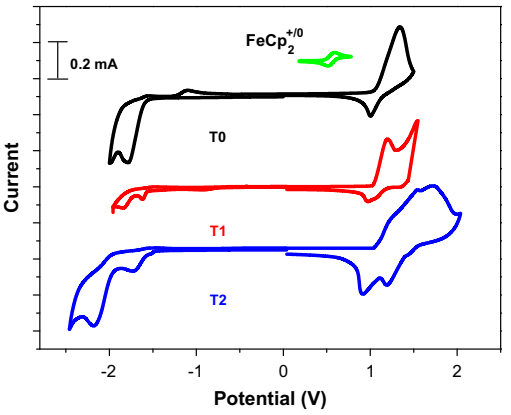

Fig. 4. Cyclic voltammograms for **T0**–**T2** in CH_3CN/0.1 M $[^nBu_4N]^+[PF_6]^-$ at 100 mV s^{-1}. The horizontal scale refers to an anodized Ag wire reference electrode.

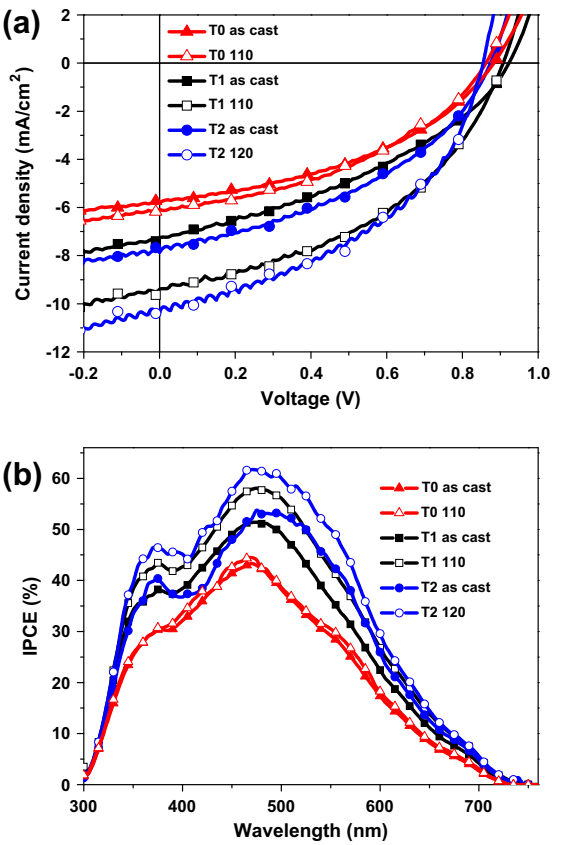

Fig. 5. *J*–*V* characteristics and IPCE curves of **T0**–**T2**/$PC_{71}BM$ (1:4, w/w) devices. (a) *J*–*V* curves of **T0**–**T2**/$PC_{71}BM$ without or with thermal annealing, and (b) IPCE spectra of **T0**–**T2**/$PC_{71}BM$ without or with thermal annealing.

9.74 mA/cm^2, 47.0% and 3.89%, respectively. The best PCE of **T2**/$PC_{71}BM$ (1:4, w/w) devices with annealing at 120 °C is 4.05%, which is higher than that (3.73%) of **T1** and is the highest for thiazole-based small molecule solar cells [32]. However, no obvious improvement in PCE was observed for **T0**/$PC_{71}BM$ (1:4, w/w) devices after thermal annealing at 110 °C for 10 min. The thermal annealing temperature slightly affects FF and V_{OC} of **T1** (or **T2**)/PC_{71}-BM (1:4, w/w) devices, but significantly affects J_{SC}, which is consistent with the trend in IPCE spectra. The J_{SC} and PCE increase first and then decrease with increasing thermal annealing temperature. After thermal annealing, the PCEs of **T0–T2**/$PC_{71}BM$ have a similar trend to those before annealing; the PCE increases with increasing thiophene number and conjugation length.

3.5. Effect of thermal annealing

We applied the method of space charge limited current (SCLC) [54] to measure hole mobility and electron mobility. Hole-only and electron-only diodes were fabricated using the architectures: ITO/PEDOT:PSS/**T0–T2**/$PC_{71}BM$ (1:4, w/w)/Au for holes and Al/**T0–T2**/$PC_{71}BM$ (1:4, w/w)/Al for electrons. The *J*–*V* curves of the devices were plotted as $\ln[Jd^3/(V_{appl}-V_{bi})^2]$ versus $[(V_{appl}-V_{bi})/d]^{0.5}$ using Eq. (1) for holes and $\ln(J)$ versus $\ln(V_{appl})$ using Eq. (2) for electrons (Fig. 6).

$$\ln\left(JL^3/V^2\right) \cong 0.89(1/E_0)^{0.5}(V/L) + \ln\left(9\varepsilon_r\varepsilon_0\mu_h/8\right) \quad (1)$$

Calculation of hole mobility using SCLC methods, $V = V_{appl}-V_{bi}$, V_{appl} is the applied voltage, V_{bi} is the offset voltage (for this device architecture, V_{bi} is 0.2 V)

$$\ln(J) = 2\ln(V) + \ln\left(9\varepsilon_r\varepsilon_0\mu_e/8L^3\right) \quad (2)$$

Calculation of electron mobility using SCLC methods, $V = V_{appl}$ (for this device architecture, V_{bi} is 0 V)

The hole mobilities, electron mobilities and ratios of electron mobility to hole mobility of **T0–T2**/$PC_{71}BM$ (1:4, w/w) without or with thermal annealing are listed in

Table 1
Thermal, optical and electrochemical data of compounds T**0**–T**2**.

Compound	T_d (°C)	λ_{max} (nm)		E_g^{opt} [a] (eV)	ε [b] (10^4 M^{-1} cm^{-1})	HOMO (eV)	LUMO (eV)	E_g^{ecc} [c] (eV)
		Solution	Film					
T0	420	430	430	2.55	2.80	−5.31	−2.64	2.67
T1	355	422	436	2.31	2.95	−5.30	−2.71	2.59
T2	385	488	492	2.11	9.40	−5.28	−2.75	2.53

[a] Estimated from the absorption edge in film.
[b] Extinction coefficient at λ_{max} in solution.
[c] Obtained from electrochemistry.

Table 2
Average and best device data at different **T0**–**T2**/$PC_{71}BM$ weight ratios without or with thermal annealing at different temperatures.

Weight ratio	Temperature (°C)	V_{OC} (V)	J_{SC} (mA cm^{-2})	FF (%)	PCE (%)	
					Average	Best
T0:$PC_{71}BM$ = 1:2	As cast	0.88	4.74	38.2	1.59	1.63
T0:$PC_{71}BM$ = 1:3	As cast	0.87	5.15	39.5	1.77	1.81
T0:$PC_{71}BM$ = 1:4	As cast	0.88	5.79	41.8	2.13	2.18
T0:$PC_{71}BM$ = 1:4	110	0.86	6.08	41.5	2.17	2.19
T1:$PC_{71}BM$ = 1:2	As cast	0.94	5.2	38.1	1.86	1.89
T1:$PC_{71}BM$ = 1:3	As cast	0.9	7.15	34.7	2.23	2.33
T1:$PC_{71}BM$ = 1:4	As cast	0.92	7.18	38.1	2.52	2.59
T1:$PC_{71}BM$ = 1:4	100	0.91	8.02	44.9	3.28	3.3
T1:$PC_{71}BM$ = 1:4	110	0.9	9.38	42.8	3.61	3.73
T1:$PC_{71}BM$ = 1:4	120	0.91	7.9	45	3.24	3.38
T1:$PC_{71}BM$ = 1:4	130	0.92	6.76	43.4	2.7	2.77
T2:$PC_{71}BM$ = 1:2	As cast	0.83	6.67	38.5	2.06	2.11
T2:$PC_{71}BM$ = 1:3	As cast	0.84	7.04	38.3	2.27	2.4
T2:$PC_{71}BM$ = 1:4	As cast	0.86	7.6	40.7	2.66	2.78
T2:$PC_{71}BM$ = 1:4	100	0.86	8.1	46.7	3.25	3.3
T2:$PC_{71}BM$ = 1:4	110	0.86	8.56	46.2	3.4	3.42
T2:$PC_{71}BM$ = 1:4	120	0.85	9.74	47	3.89	4.05
T2:$PC_{71}BM$ = 1:4	130	0.85	7.83	45.5	3.03	3.09

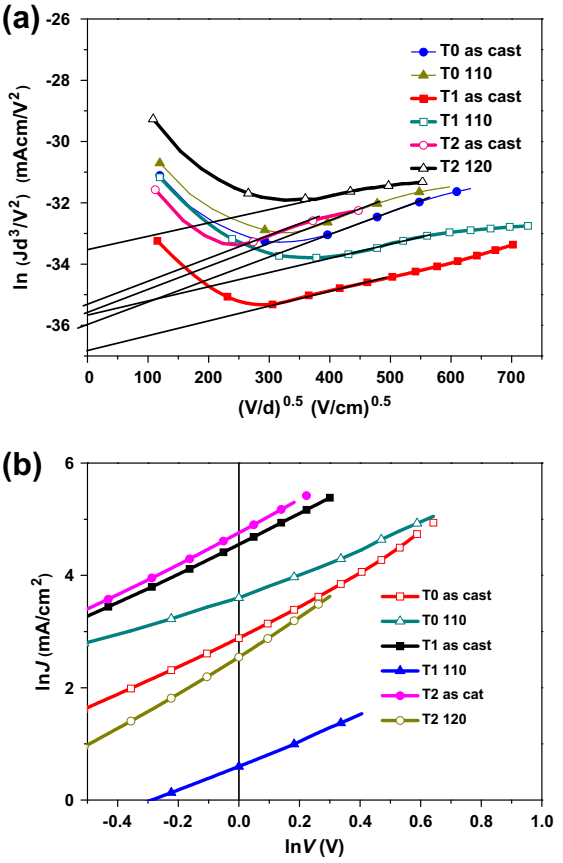

Fig. 6. Measured *J*–*V* characteristics under dark for (a) hole-only, and (b) electron-only devices based on blend films of **T0**–**T2**/$PC_{71}BM$ (1:4, w/w) without or with thermal annealing.

Table 3. As-cast film of **T0–T2**/$PC_{71}BM$ (1:4, w/w) exhibits a hole mobility ranging from 3.66×10^{-7} to 1.70×10^{-6} $cm^2\,V^{-1}\,s^{-1}$ and an electron mobility ranging from

Table 3
The hole mobilities, electron mobilities and ratios of electron mobility to hole mobility of T0–T2/$PC_{71}BM$ (1:4, w/w) without or with thermal annealing.

Blend	Annealing (°C)	μ_h ($cm^2\,V^{-1}\,s^{-1}$)	μ_e ($cm^2\,V^{-1}\,s^{-1}$)	μ_e/μ_h
T0:$PC_{71}BM$	As cast	8.31×10^{-7}	1.71×10^{-5}	20.58
T0:$PC_{71}BM$	110	1.37×10^{-6}	3.81×10^{-5}	27.81
T1:$PC_{71}BM$	As cast	3.66×10^{-7}	1.03×10^{-4}	281.42
T1:$PC_{71}BM$	110	1.28×10^{-6}	3.02×10^{-6}	2.36
T2:$PC_{71}BM$	As cast	1.70×10^{-6}	1.13×10^{-4}	66.47
T2:$PC_{71}BM$	120	1.01×10^{-5}	1.89×10^{-5}	1.89

1.71×10^{-5} to 1.13×10^{-4} $cm^2\,V^{-1}\,s^{-1}$. The electron mobility is ca. 2 orders of magnitude higher than the hole mobility. The unbalanced electron and hole transport is partially responsible for the relatively low PCE. After thermal annealing, the hole mobility of **T0–T2**/$PC_{71}BM$ (1:4, w/w) increases by 1 order of magnitude (1.28×10^{-6} to 1.01×10^{-5} $cm^2\,V^{-1}\,s^{-1}$), while the electron mobility of **T1–T2**/$PC_{71}BM$ (1:4, w/w) decreases by 1 to 2 orders of magnitude (3.02×10^{-6} to 1.89×10^{-5} $cm^2\,V^{-1}\,s^{-1}$). The more balanced electron and hole transport is beneficial to the efficiency enhancement. In particular, **T2**/$PC_{71}BM$ (1:4, w/w) blend film exhibits high and balanced electron mobility (1.89×10^{-5} $cm^2\,V^{-1}\,s^{-1}$) and hole mobility (1.01×10^{-5} $cm^2\,V^{-1}\,s^{-1}$), leading to the best photovoltaic performance.

Fig. 7 shows the atomic force microscope (AFM) images of **T0–T2**/$PC_{71}BM$ (1:4, w/w) films before and after thermal annealing. The blend films exhibit a typical cluster structure with many aggregated domains and a root-mean-square (RMS) roughness of 0.363, 0.376 and 0.385 nm, respectively. After thermal annealing, RMS roughness of the **T0**/$PC_{71}BM$ blend film increases to 0.384 nm, while RMS roughness of the **T1–T2**/$PC_{71}BM$ blend film decreases to 0.368 and 0.314 nm, respectively. The more uniform and smooth film of **T1–T2**/$PC_{71}BM$ blend leads to improved FF. The larger aggregated domains lead to smaller donor/acceptor interfacial area. Moreover, given the fact that

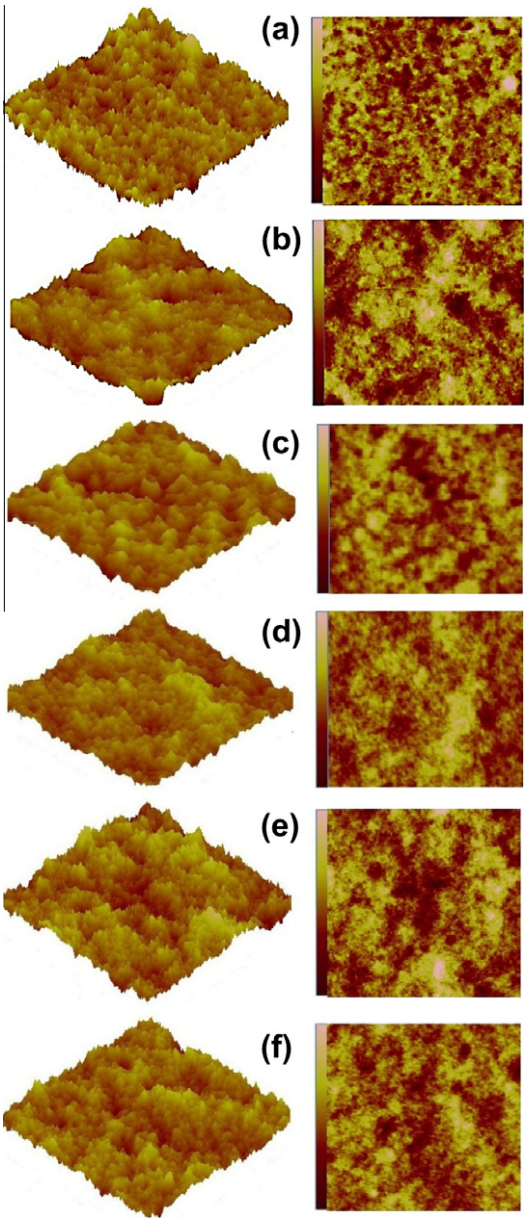

Fig. 7. AFM height images of **T0**–**T2**/$PC_{71}BM$ (1:4, w/w) films spin-coated on ITO/PEDOT:PSS substrates: **T0**/$PC_{71}BM$ as-cast (a), **T0**/$PC_{71}BM$ annealing at 110 °C (b), **T1**/$PC_{71}BM$ as-cast (c), **T1**/$PC_{71}BM$ annealing at 110 °C (d), **T2**/$PC_{71}BM$ as-cast (e), and **T2**/$PC_{71}BM$ annealing at 120 °C (f). The scale of height images are 0–3 nm. The scan size for all images is 3 μm × 3 μm.

typical exciton diffusion length in disordered blend layer is about 10 nm, the larger scale phase separation in **T1–T2**/$PC_{71}BM$ (1:4, w/w) blend before thermal annealing is not favorable for efficient exciton dissociation, leading to lower J_{SC}, IPCE and PCE compared to that after thermal annealing.

4. Conclusions

Small molecule donors **T0–T2** with thiazolothiazole as acceptor unit, TPA as donor unit and thiophene with different number as bridge were synthesized. With increasing thiophene number and conjugation length, these molecules exhibit red-shifted and enhanced absorption, up-shifted HOMO level, down-shifted LUMO level, and reduced band gap. Solution processed OSCs based on **T0–T2**/$PC_{71}BM$ (1:4, w/w) exhibit average PCE of 2.13%, 2.52% and 2.66%, respectively; the J_{SC}, IPCE and PCE increase with increasing thiophene number and conjugation length, due to red-shifted and enhanced absorption as well as enhanced hole mobility. After thermal annealing, **T0**/$PC_{71}BM$ (110 °C), **T1**/$PC_{71}BM$ (110 °C), and **T2**/$PC_{71}BM$ (120 °C) based devices exhibit average PCE of 2.17%, 3.61% and 3.89%, respectively. Thermal annealing leads to suitable aggregation domain and phase separation scale, balanced hole and electron transport and finally improved photovoltaic performance.

Acknowledgements

We thank the NSFC (21025418, 51011130028, 21021091), the 973 Project (2011CB808401), and the Chinese Academy of Sciences for financial support.

References

[1] S. Gunes, H. Neugebauer, N. Sariciftci, Chem. Rev. 107 (2007) 1324.
[2] Y. Li, Acc. Chem. Res. 45 (2012) 723.
[3] X. Zhan, D. Zhu, Polym. Chem. 1 (2010) 409.
[4] G. Dennler, M. Scharber, C. Brabec, Adv. Mater. 21 (2009) 1323.
[5] Y. Cheng, S. Yang, C. Hsu, Chem. Rev. 109 (2009) 5868.
[6] G. Li, R. Zhu, Y. Yang, Nat. Photonics 6 (2012) 153.
[7] H. Chen, J. Hou, S. Zhang, Y. Liang, G. Yang, Y. Yang, L. Yu, Y. Wu, G. Li, Nat. Photonics 3 (2009) 649.
[8] Z. He, C. Zhong, S. Su, M. Xu, H. Wu, Y. Cao, Nat. Photonics 6 (2012) 591.
[9] T. Chu, J. Lu, S. Beaupré, Y. Zhang, J. Pouliot, S. Wakim, J. Zhou, M. Leclerc, Z. Li, J. Ding, Y. Tao, J. Am. Chem. Soc. 133 (2011) 4250.
[10] H. Son, W. Wang, T. Xu, Y. Liang, Y. Wu, G. Li, L. Yu, J. Am. Chem. Soc. 133 (2011) 1885.
[11] T.B. Yang, M. Wang, C.H. Duan, X.W. Hu, L. Huang, J.B. Peng, F. Huang, X. Gong, Energy Environ. Sci. 5 (2012) 8208.
[12] H. Zhou, L. Yang, A. Stuart, S. Price, S. Liu, W. You, Angew. Chem. Int. Edit. 50 (2011) 2995.
[13] Z. He, C. Zhong, X. Huang, W. Wong, H. Wu, L. Chen, S. Su, Y. Cao, Adv. Mater. 23 (2011) 4636.
[14] L. Dou, J. You, J. Yang, C. Chen, Y. He, S. Murase, T. Moriarty, K. Emery, G. Li, Y. Yang, Nat. Photonics 6 (2012) 180.
[15] X. Li, W. Choy, L. Huo, F. Xie, W. Sha, B. Ding, X. Guo, Y. Li, J. Hou, J. You, Y. Yang, Adv. Mater. 24 (2012) 3046.
[16] Y. Lin, Y. Li, X. Zhan, Chem. Soc. Rev. 41 (2012) 4245.
[17] A. Mishra, P. Bäuerle, Angew. Chem. Int. Edit. 51 (2012) 2020.
[18] A. Hains, Z. Liang, M. Woodhouse, B. Gregg, Chem. Rev. 110 (2010) 6689.
[19] B. Walker, C. Kim, T. Nguyen, Chem. Mater. 23 (2011) 470.
[20] Y. Li, Q. Guo, Z. Li, J. Pei, W. Tian, Energy Environ. Sci. 3 (2010) 1427.
[21] J. Roncali, Acc. Chem. Res. 42 (2009) 1719.
[22] B. Walker, A. Tamayo, X. Dang, P. Zalar, J. Seo, A. Garcia, M. Tantiwiwat, T. Nguyen, Adv. Funct. Mater. 19 (2009) 3063.
[23] H. Shang, H. Fan, Y. Liu, W. Hu, Y. Li, X. Zhan, Adv. Mater. 23 (2011) 1554.
[24] Y. Liu, X. Wan, F. Wang, J. Zhou, G. Long, J. Tian, Y. Chen, Adv. Mater. 23 (2011) 5387.
[25] V.N. Steinmann, M. Kronenberg, M.R. Lenze, S.M. Graf, D. Hertel, K. Meerholz, H. Bürckstümmer, E.V. Tulyakova, F. Würthner, Adv. Energy Mater. 1 (2011) 888.
[26] N. Zhou, X. Guo, R. Ortiz, S. Li, S. Zhang, R. Chang, A. Facchetti, T. Marks, Adv. Mater. 24 (2012) 2242.
[27] Z. Li, G. He, X. Wan, Y. Liu, J. Zhou, G. Long, Y. Zuo, M. Zhang, Y. Chen, Adv. Energy Mater. 2 (2012) 74.
[28] S.-W. Chiu, L.-Y. Lin, H.-W. Lin, Y.-H. Liu, Z.-Y. Huang, Y.-T. Lin, F. Lin, Y.-H. Chen, K.-T. Wong, Chem. Commun. 48 (2012) 1857.

[29] Y. Sun, G. Welch, W. Leong, C. Takacs, G. Bazan, A. Heeger, Nat. Mater. 11 (2012) 44.
[30] T.S. Van der Poll, J.A. Love, T.-Q. Nguyen, G.C. Bazan, Adv. Mater. 24 (2012) 3646.
[31] J. Zhou, X. Wan, Y. Liu, Y. Zuo, Z. Li, G. He, G. Long, W. Ni, C. Li, X. Su, Y. Chen, J. Am. Chem. Soc. 134 (2012) 16345.
[32] Y. Lin, H. Fan, Y. Li, X. Zhan, Adv. Mater. 24 (2012) 3087.
[33] Q. Shi, H. Fan, Y. Liu, W. Hu, Y. Li, X. Zhan, J. Phys. Chem. C 114 (2010) 16843.
[34] M. Zhang, X. Guo, Y. Li, Adv. Energy Mater. 1 (2011) 557.
[35] Z.-G. Zhang, J. Min, S. Zhang, J. Zhang, M. Zhang, Y. Li, Chem. Commun. 47 (2011) 9474.
[36] Q. Shi, H. Fan, Y. Liu, W. Hu, Y. Li, X. Zhan, Macromolecules 44 (2011) 9173.
[37] L. Huo, X. Guo, S. Zhang, Y. Li, J. Hou, Macromolecules 44 (2011) 4035.
[38] M. Zhang, Y. Sun, X. Guo, C. Cui, Y. He, Y. Li, Macromolecules 44 (2011) 7625.
[39] M. Zhang, X. Guo, X. Wang, H. Wang, Y. Li, Chem. Mater. 23 (2011) 4264.
[40] Q. Shi, H. Fan, Y. Liu, J. Chen, Z. Shuai, W. Hu, Y. Li, X. Zhan, J. Polym. Sci., Part A: Polym. Chem. 49 (2011) 4875.
[41] I. Osaka, M. Saito, H. Mori, T. Koganezawa, K. Takimiya, Adv. Mater. 24 (2012) 425.
[42] A. Bhuwalka, J.F. Mike, M. He, J.J. Intemann, T. Nelson, M.D. Ewan, R.A. Roggers, Z. Lin, M. Jeffries -El, Macromolecules 44 (2011) 9611.
[43] I.H. Jung, J. Yu, E. Jeong, J. Kim, S. Kwon, H. Kong, K. Lee, H.Y. Woo, H.K. Shim, Chem. -Eur. J. 16 (2010) 3743.
[44] S.K. Lee, J.M. Cho, Y. Goo, W.S. Shin, J.-C. Lee, W.-H. Lee, I.-N. Kang, H.-K. Shim, S.-J. Moon, Chem. Commun. 47 (2011) 1791.
[45] T.W. Lee, N.S. Kang, J. Yu, M.H. Hoang, K.H. Kim, J.-I. Jin, D.H. Choi, J. Polym. Sci., Part A: Polym. Chem. 48 (2010) 5921.
[46] S. Subramaniyan, H. Xin, F.S. Kim, S.A. Jenekhe, Macromolecules 44 (2011) 6245.
[47] S. Subramaniyan, H. Xin, F.S. Kim, S. Shoaee, J.R. Durrant, S.A. Jenekhe, Adv. Energy Mater. 1 (2011) 854.
[48] S. Van Mierloo, A. Hadipour, M.-J. Spijkman, N. Van den Brande, B. Ruttens, J. Kesters, J. D'Haen, G. Van Assche, D.M. de Leeuw, T. Aernouts, J. Manca, L. Lutsen, D.J. Vanderzande, W. Maes, Chem. Mater. 24 (2012) 587.
[49] Q. Shi, P. Cheng, Y. Li, X. Zhan, Adv. Energy Mater. 2 (2012) 63.
[50] P. Dutta, W. Yang, S.H. Eom, S.-H. Lee, Org. Electron. 13 (2012) 273.
[51] P. Dutta, H. Park, W.-H. Lee, I.-N. Kang, S.-H. Lee, Org. Electron. 13 (2012) 3183.
[52] J. Liu, X. Guo, L. Bu, Z. Xie, Y. Cheng, Y. Geng, L. Wang, X. Jing, F. Wang, Adv. Funct. Mater. 17 (2007) 1917.
[53] I. Osaka, G. Sauvé, R. Zhang, T. Kowalewski, R. McCullough, Adv. Mater. 19 (2007) 4160.
[54] G. Malliaras, J. Salem, P. Brock, C. Scott, Phys. Rev. B 58 (1998) 13411.